

Advantage and disadvantage of LHD heliotron divertor

M. Kobayashi, T. Goto, Y. Hayashi, G. Kawamura, G. Motojima, S. Morita, K. Mukai, S. Masuzaki, T. Oishi, C. Suzuki, T. Morisaki, and the LHD experimental group

National Institute for Fusion Science

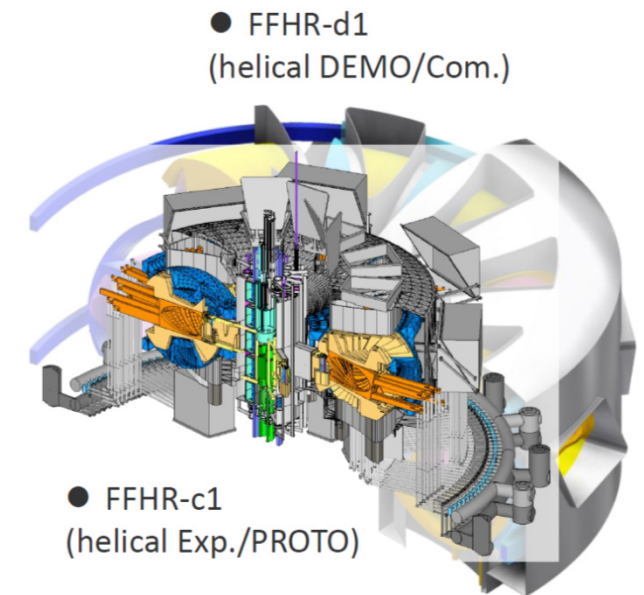
Outline of the talk

1. Introduction: divertor optimization toward DEMO
2. The divertor geometry of LHD heliotron
3. Particle exhaust
4. Impurity screening
5. Power exhaust
6. Summary and discussion

Introduction: Optimization of divertor functions toward helical DEMO

Divertor functions:

1. Pumping
Effects of 3D geometry of divertor structure on neutral compression and manufacturing of pumping system
2. Impurity control
Role of edge stochastic layer on impurity screening
3. Heat load mitigation
Divertor heat load distribution in the 3D divertor structure, Detachment stability with the edge stochastic layer
4. Compatibility with core plasma performance?



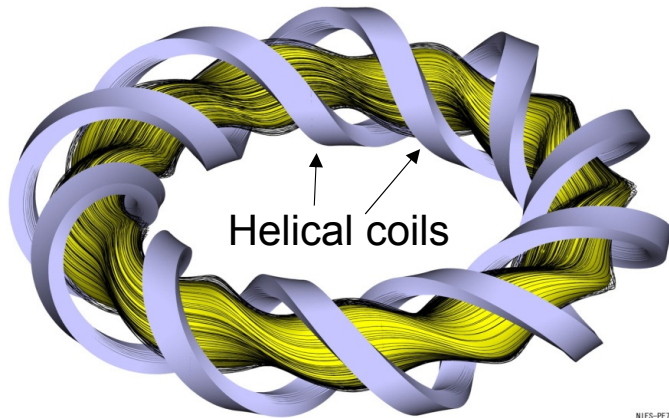
This contribution presents current achievements and understandings of LHD heliotron divertor, for further discussion of critical issues for divertor optimization toward helical DEMO.

	FFHR-d1 (DEMO)	ITER	JA Tokamak DEMO ^[5] ** w/ increasing elongation and seeding
R / a [m]	15.6 / 2.5	6.2 / 2.0	8.5 / 2.42
B_c [T]	~5	5.3	5.94
P_{fus} [MW]	3000	500	1462 (1694)**
f_{He} / f_{Ar} [%]	5 / 0	<5 / NA	7 / 0.25 (0.6)**
P_{rad} [MW]	200	~70	82 (177)**
P_{aux} [MW]	0	73	84 (96)**
$P_{div} (= P_{\alpha} + P_{aux} - P_{rad})$ [MW]	400	~100	294 (258)**
P_{div}/R [MW/m]	35	16	35 (30)**

The divertor geometry of LHD heliotron divertor

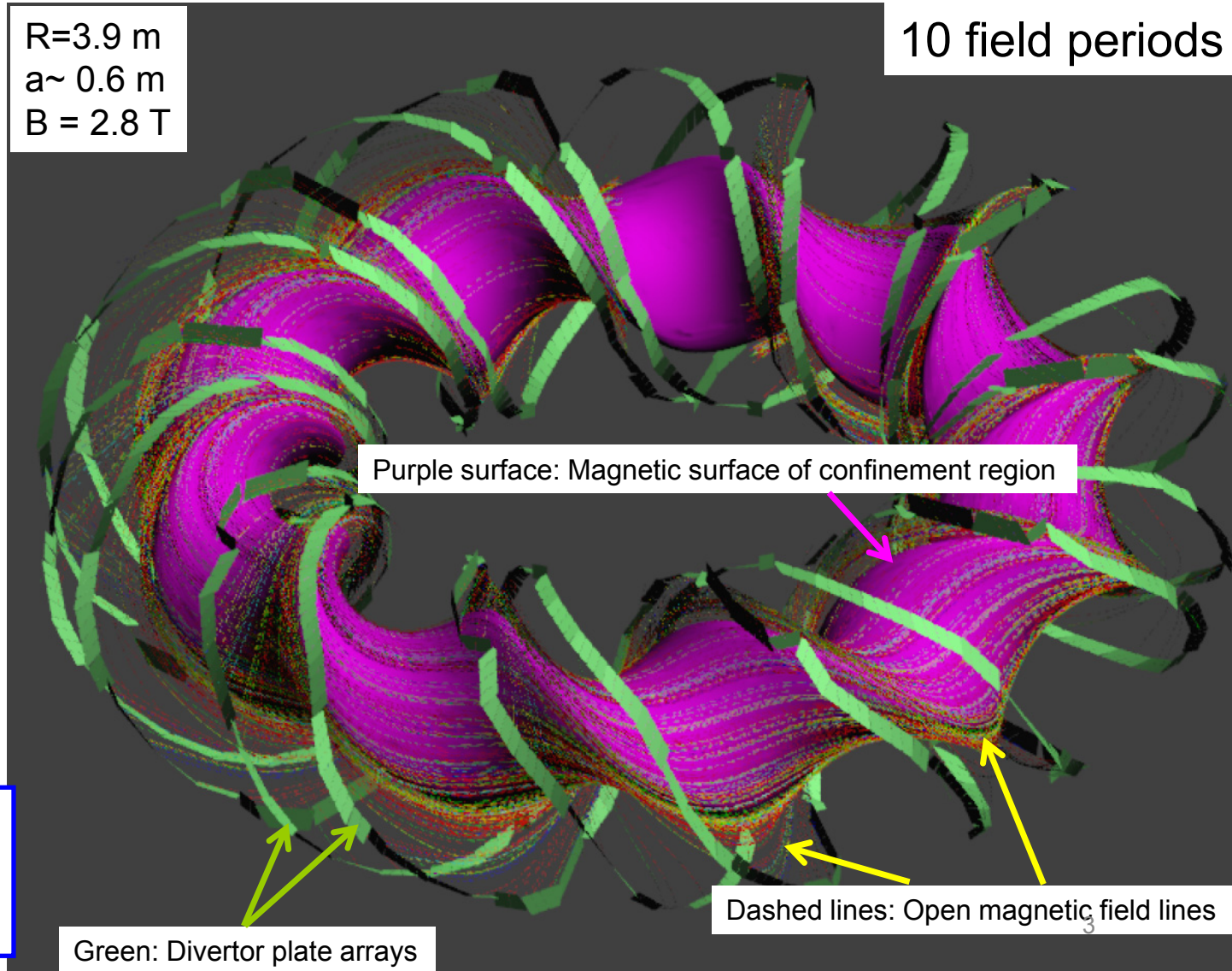
Heliotron

(Helios: the god of the sun in Greek mythology)



$R=3.9$ m
 $a\sim 0.6$ m
 $B = 2.8$ T

10 field periods



Purple surface: Magnetic surface of confinement region

Dashed lines: Open magnetic field lines

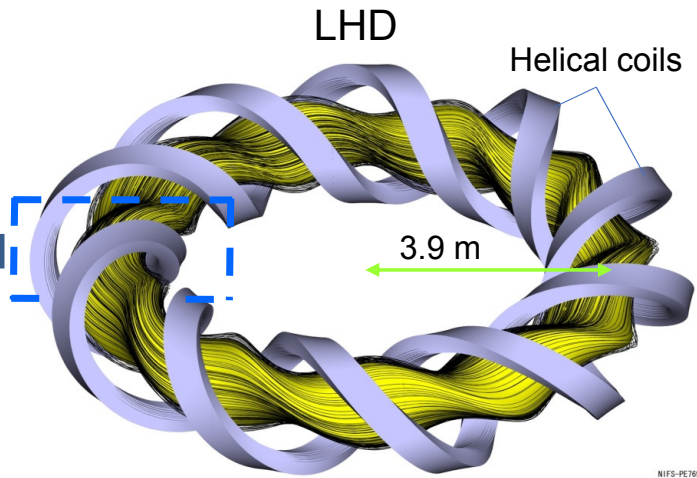
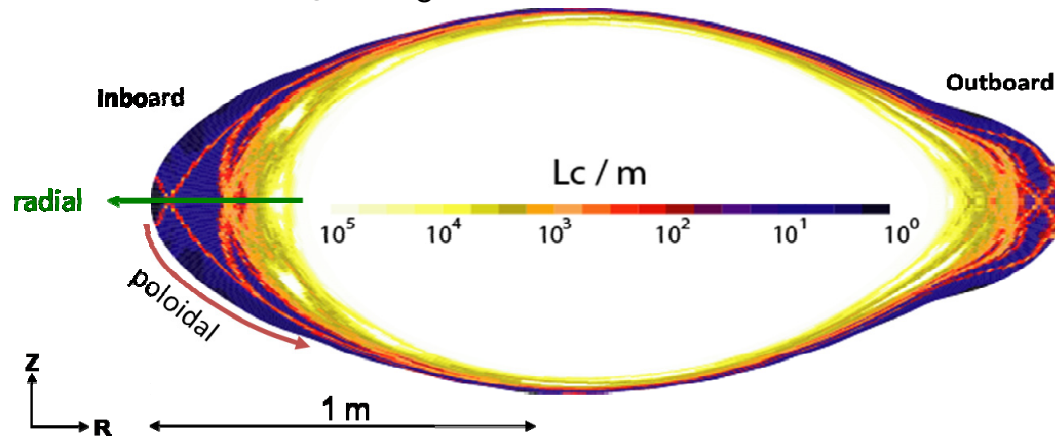
Green: Divertor plate arrays

Heating Systems

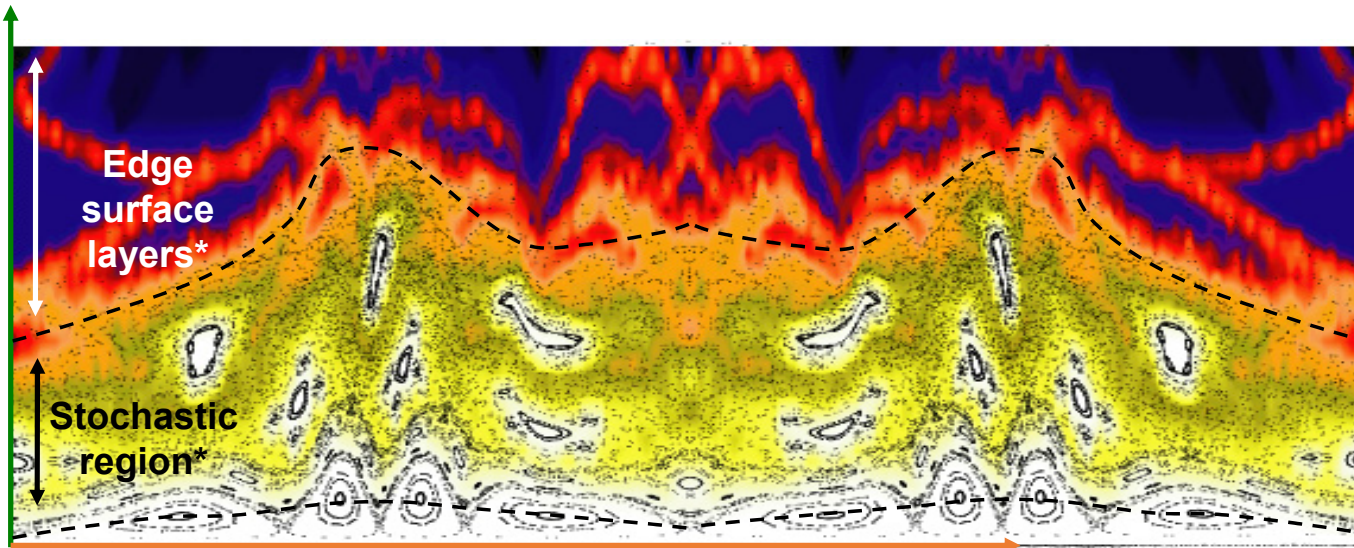
- n-NBI x 3 (180-190keV), H16MW, D8MW
- p-NBI x 2 (40-80keV), H6MW, D18MW
- ECH (77GHz x 3, 154 x 2, 82.7, 84) 5.5MW

Formation of edge stochastic layers : island chains of various modes

Connection length (L_C) distribution in poloidal cross section



radial



Mode structure
n/m

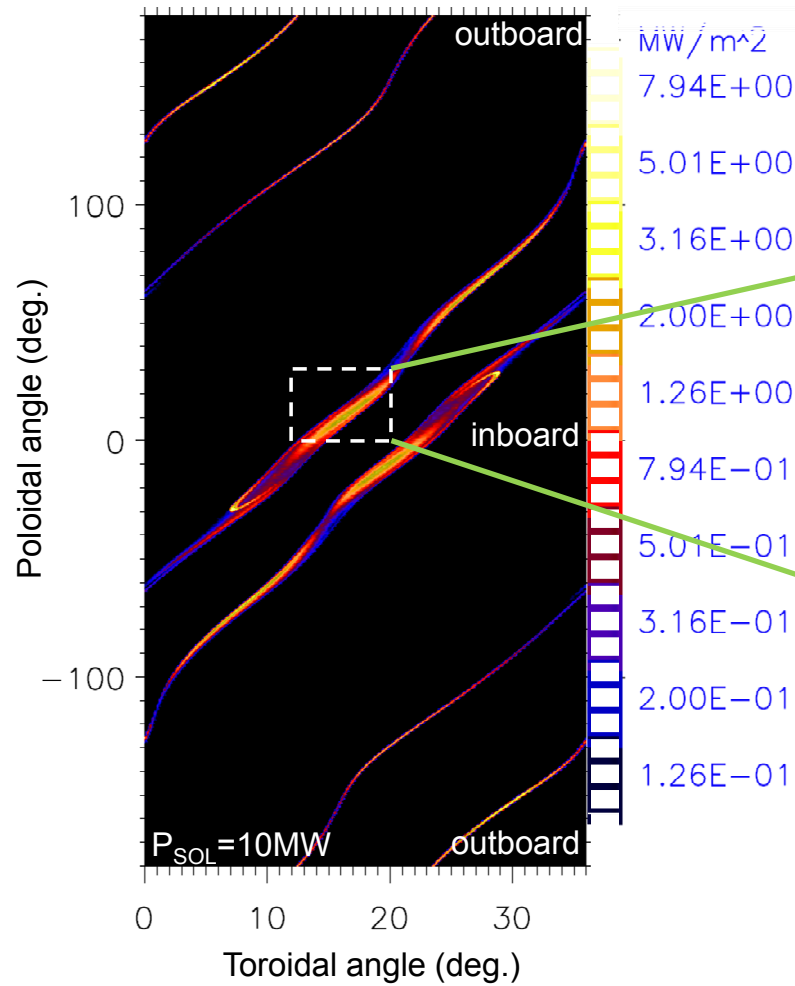
- 10/2
- 10/3
- 10/4
- 10/5
- 10/6
- 10/7
- 10/8

poloidal

Particle exhaust in LHD helical divertor

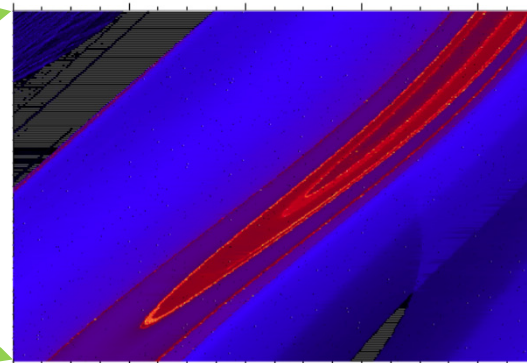
Non-uniform plasma heat/particle deposition at divertor plates

Divertor heat load distribution (EMC3-EIRENE)

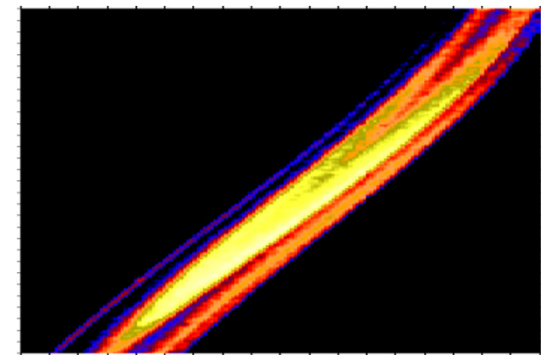


The divertor heat (particle) load distribution is not uniform in helical direction.
The heat load tends to localize at inboard side (and up & bottom).

Magnetic footprint at divertor plate



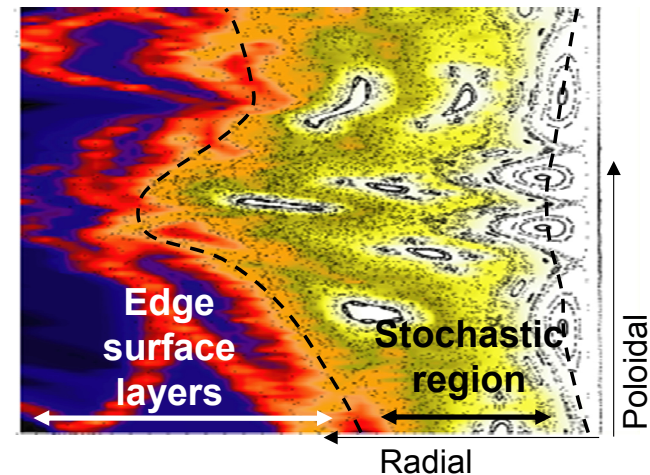
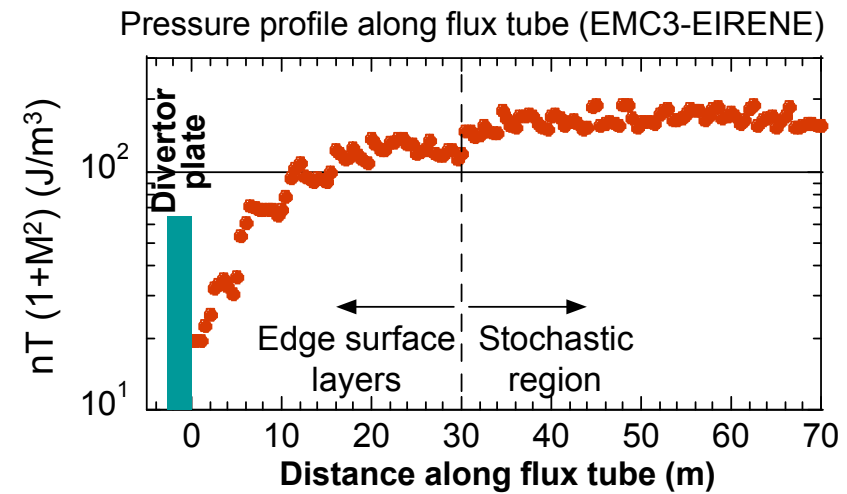
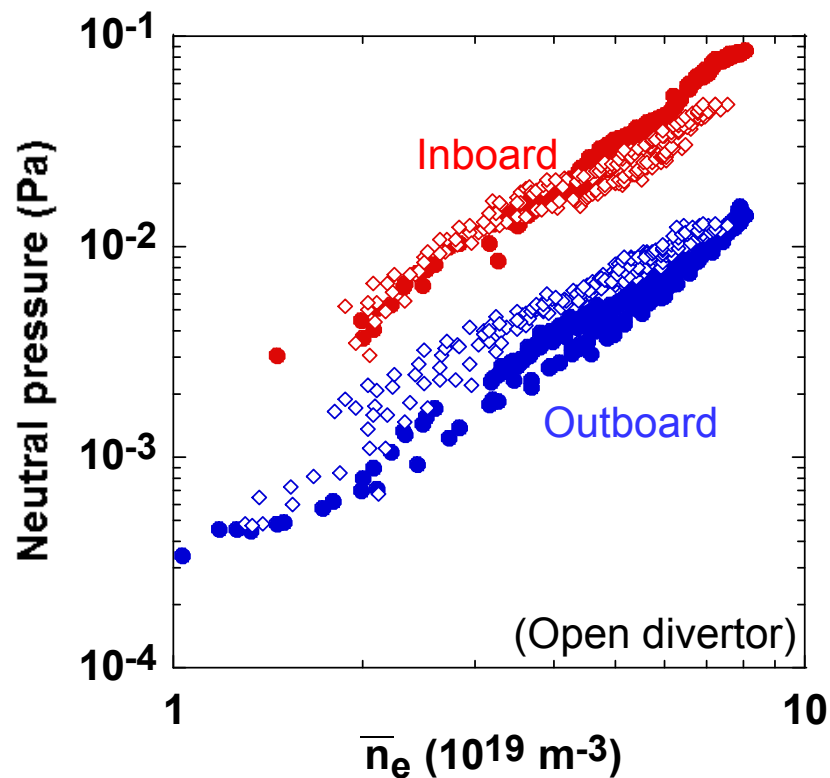
Divertor heat load distribution (EMC3-EIRENE)



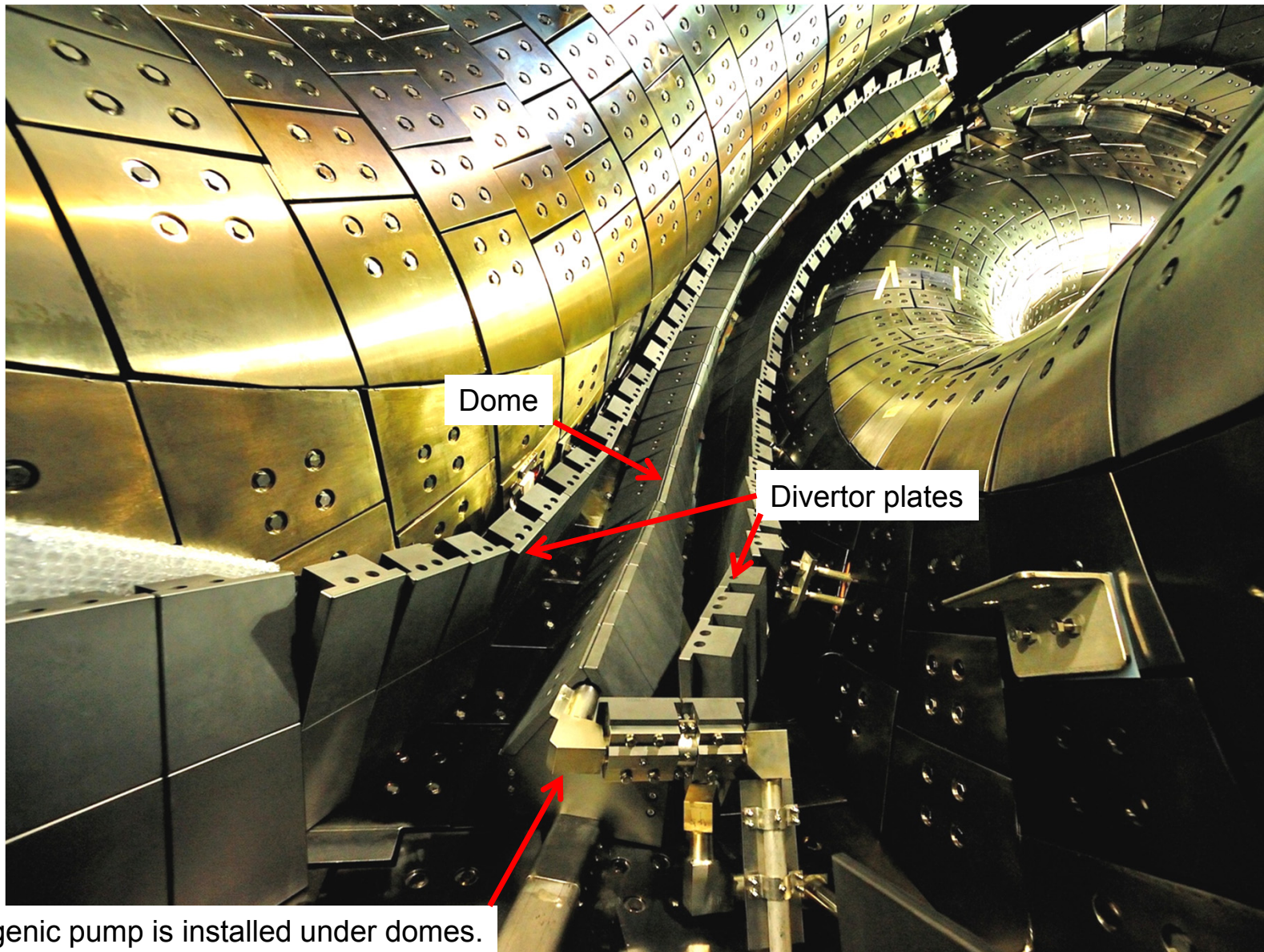
Correlation with L_c distribution is observed

In-out asymmetry of divertor neutral pressure

- Higher inboard neutral pressure than outboard by one order of magnitude.
- The rather low pressure (0.01 ~ 0.1 Pa) is due to low divertor density, $< 1 \times 10^{19} \text{ m}^{-3}$ (Absence of high recycling regime).
 - ← loss of pressure conservation along flux tubes due to enhanced cross-field transport (3D effect).

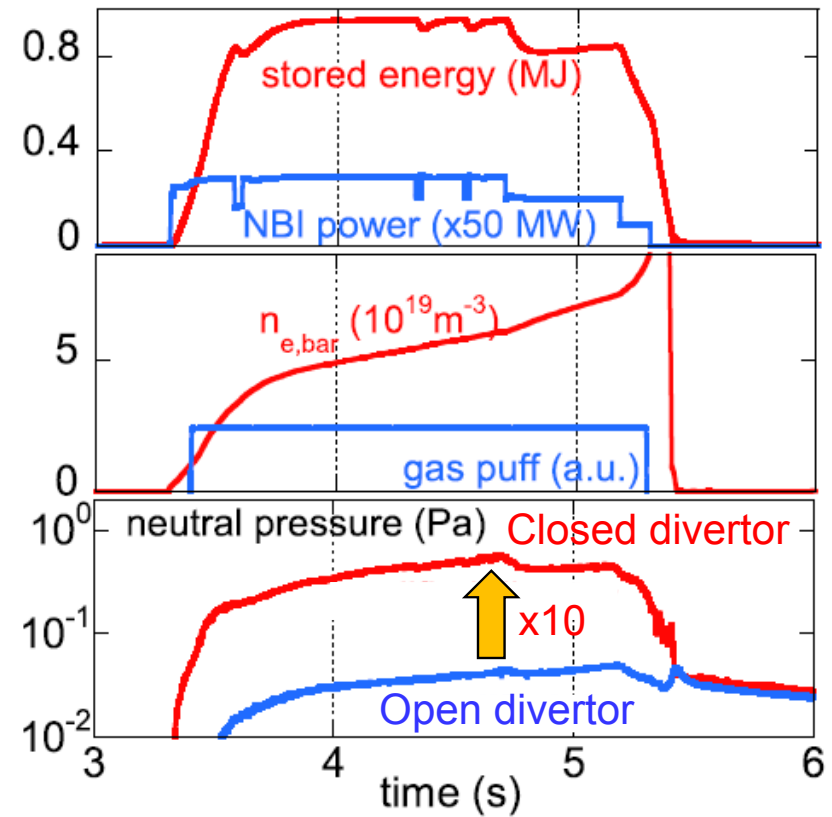
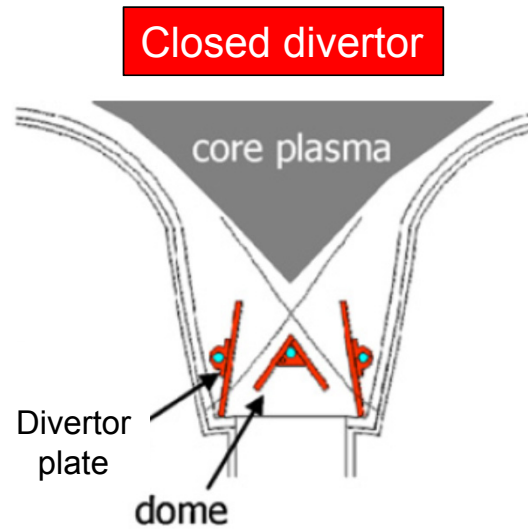
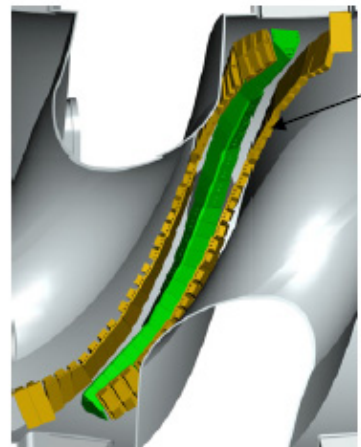
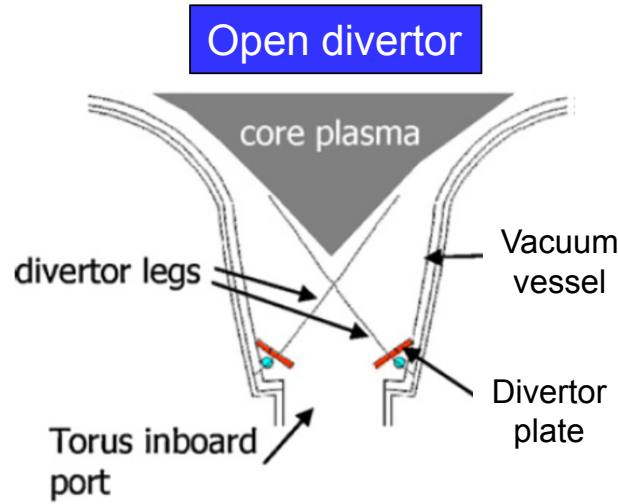
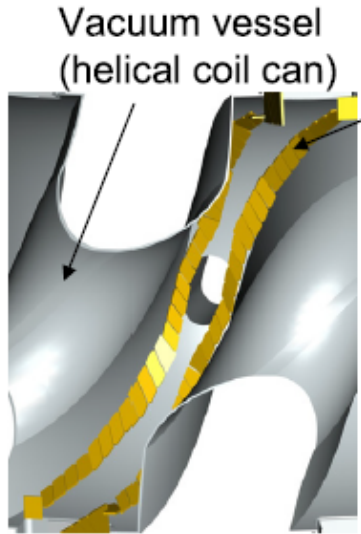


Closed Divertor since 2010

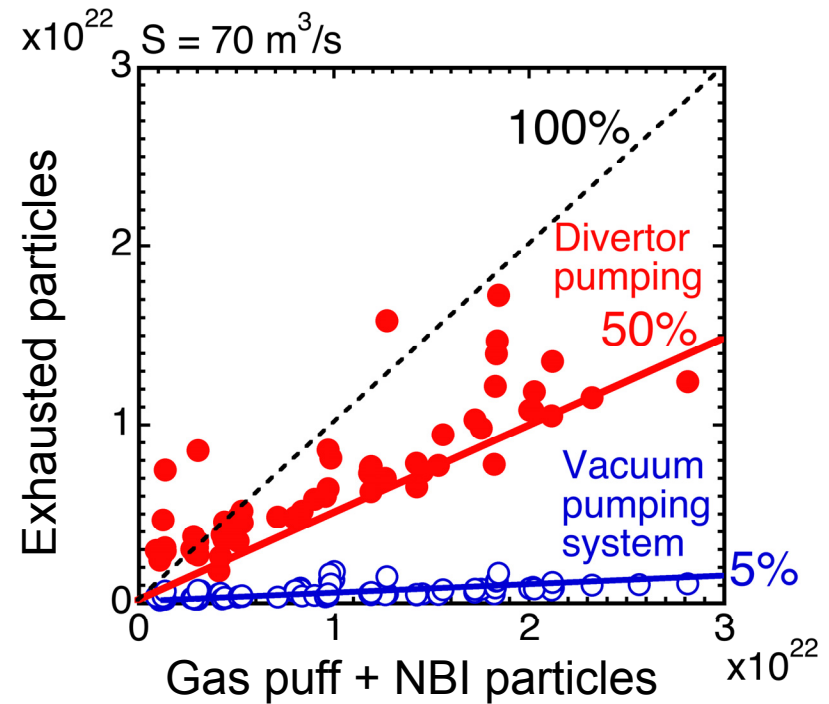
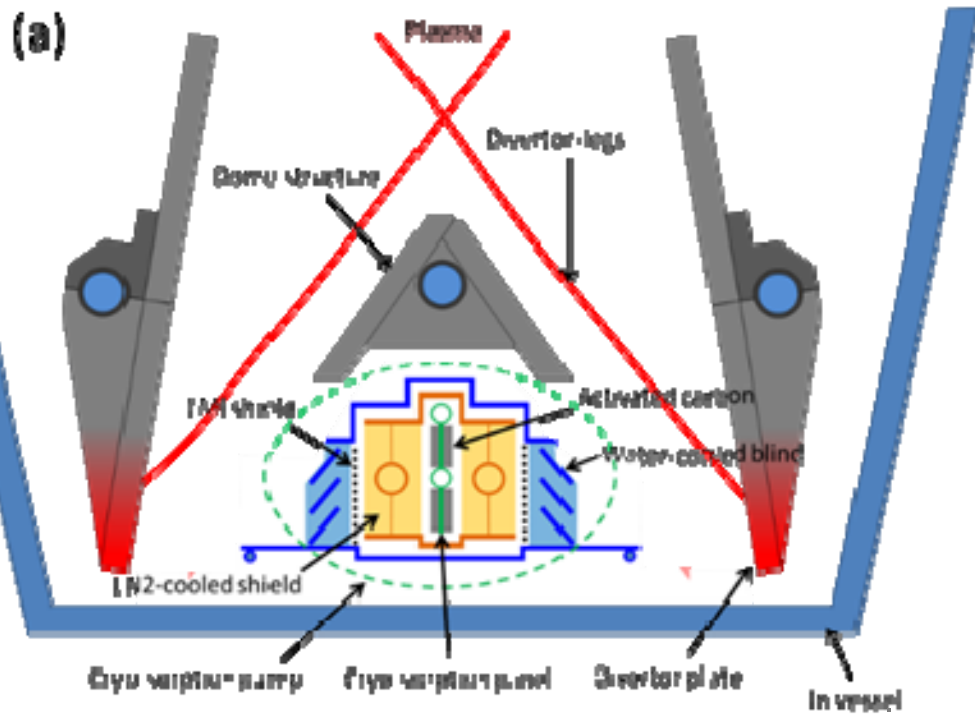


Cryogenic pump is installed under domes.

Closed divertor successfully increases divertor neutral pressure by a factor of ~10



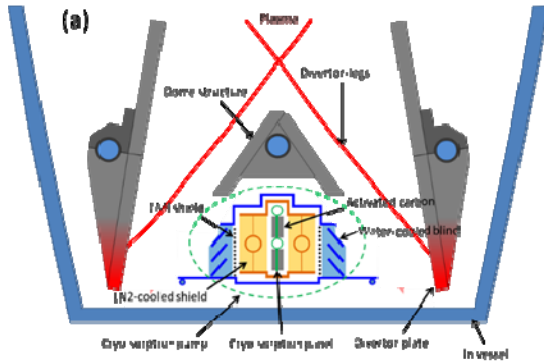
Particle exhaust with the divertor pump installed under the dome structure



- ✓ Approximately 50% of the fueled gas is exhausted in the divertor pumping.
- ✓ Slight degradation of pumping efficiency observed in high density range.

Development of divertor cryo-sorption pump in 3D geometry

Old prototype

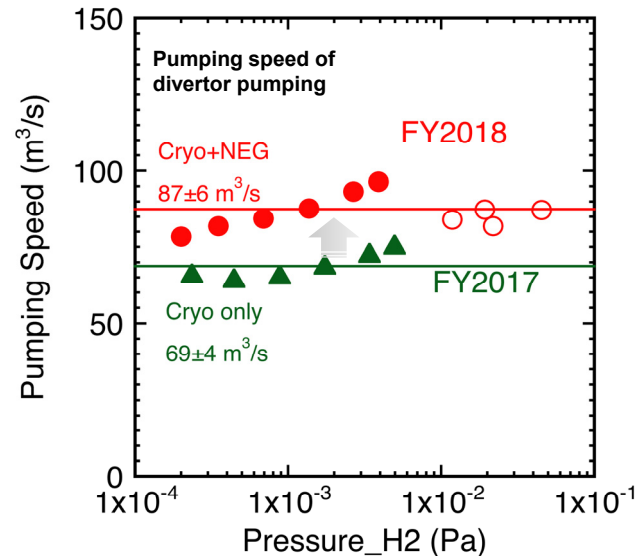


The main characteristics of the development:

- (1) Development of new activated cryo-panel → high pump speed and capacity
- (2) The water-cooled blinds are no longer needed → high conductance
- (3) The area of the cryo-sorption panel is enlarged → high capacity

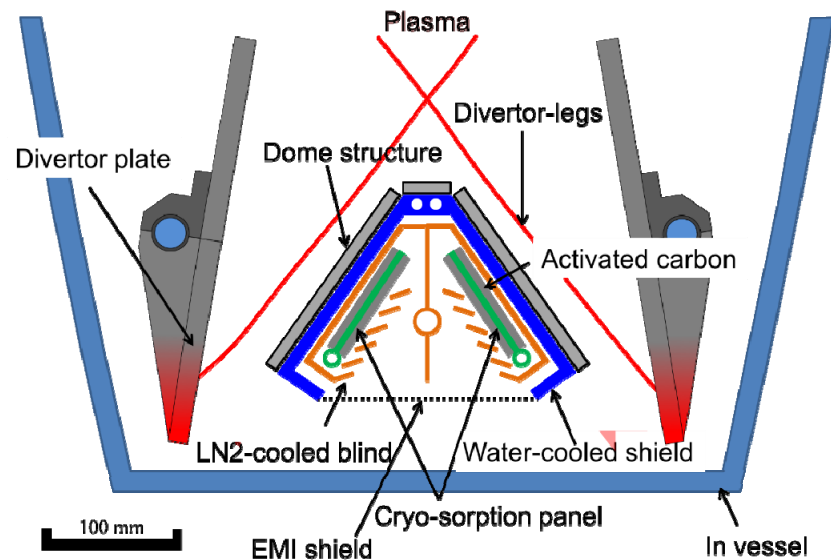


3D shaping and compactness



G. Motojima IAEA 2018.

New type

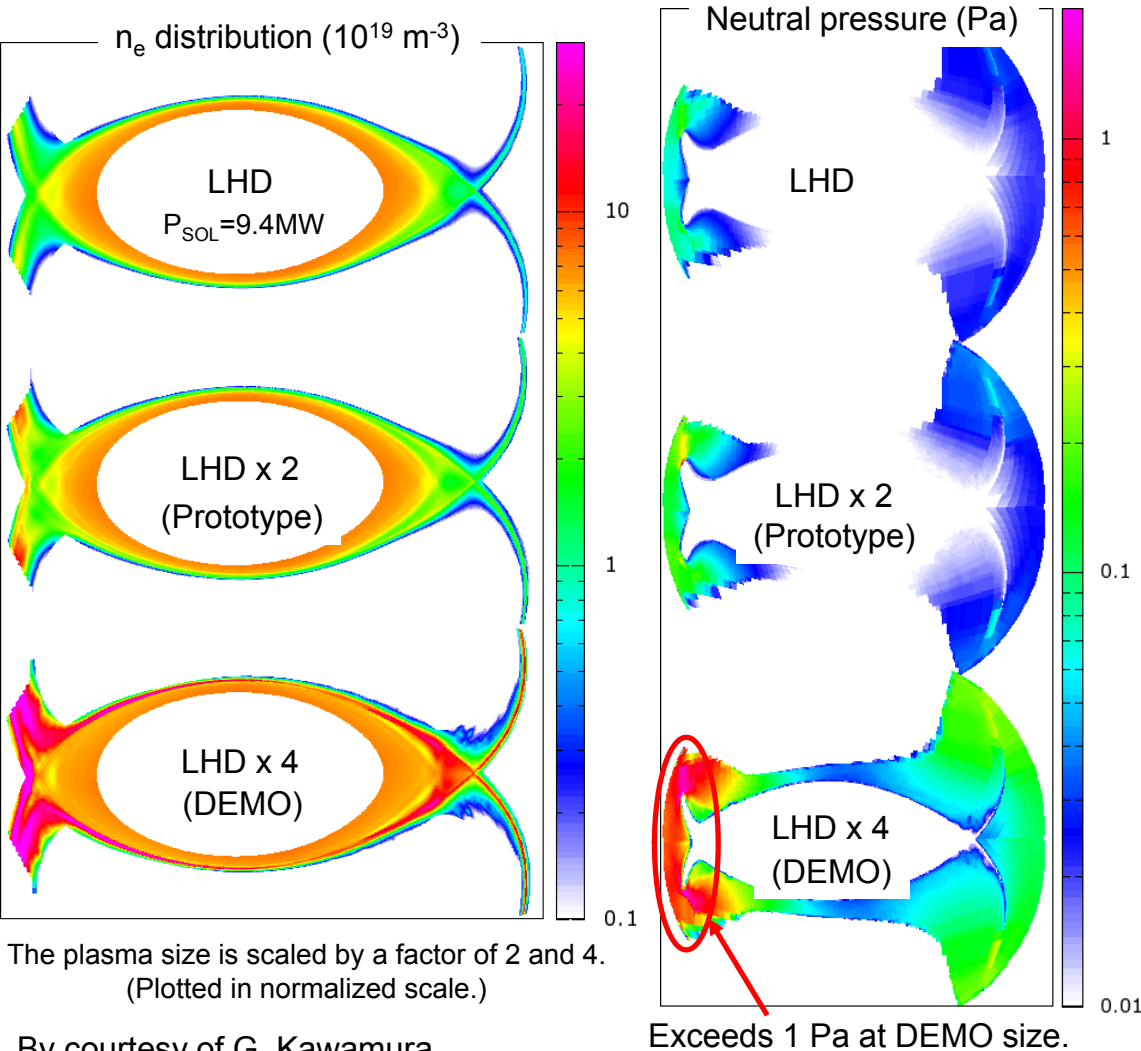


Pumping speed of 96.5 m³/s, capacity of 86,000 Pa m³ have been achieved so far. To be operated in next experiments.

T. Murase *et al.*, Plasma. Fus. Res. 11, (2016) 1205030.

Prediction of particle exhaust in helical DEMO

Prediction of EMC3-EIRENE for size-scaled computation (*Preliminary*)



	LHD	LHD x 2 (Prototype)	LHD x 4 (DEMO)
R_{ax} (m)	3.6	7.2	14.4
D/χ (m^2/s)	0.5/1.0	0.5/1.0	0.5/1.0
n_{up} (10^{19} m^{-3})	7	7	7
P_{SOL} (MW)	9.4	75	600

Prediction of EMC3-EIRENE with simply size-scaled computations shows increase in divertor density and neutral pressure

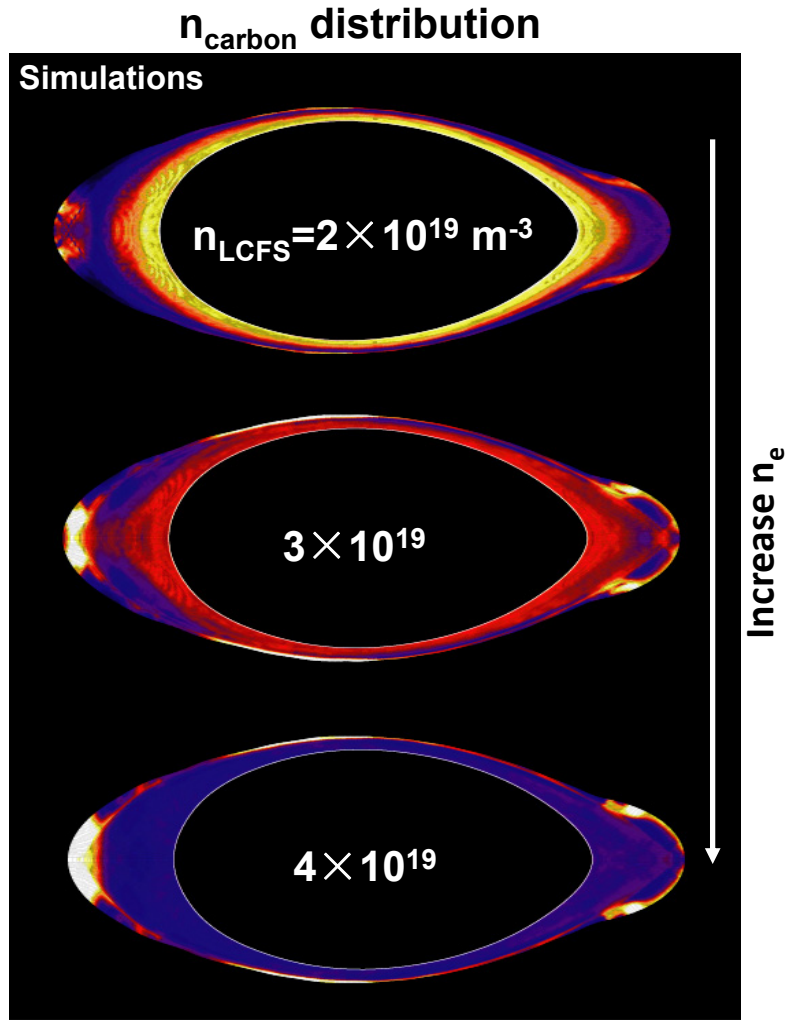
← due to change of relative scale of neutral mfp against plasma size + higher plasma pressure

The results suggest favorable situation for divertor pumping.

Combination with outboard pumping will improve the pumping efficiency further.
Replacement of cryogenic pump to TMP will be an issue.

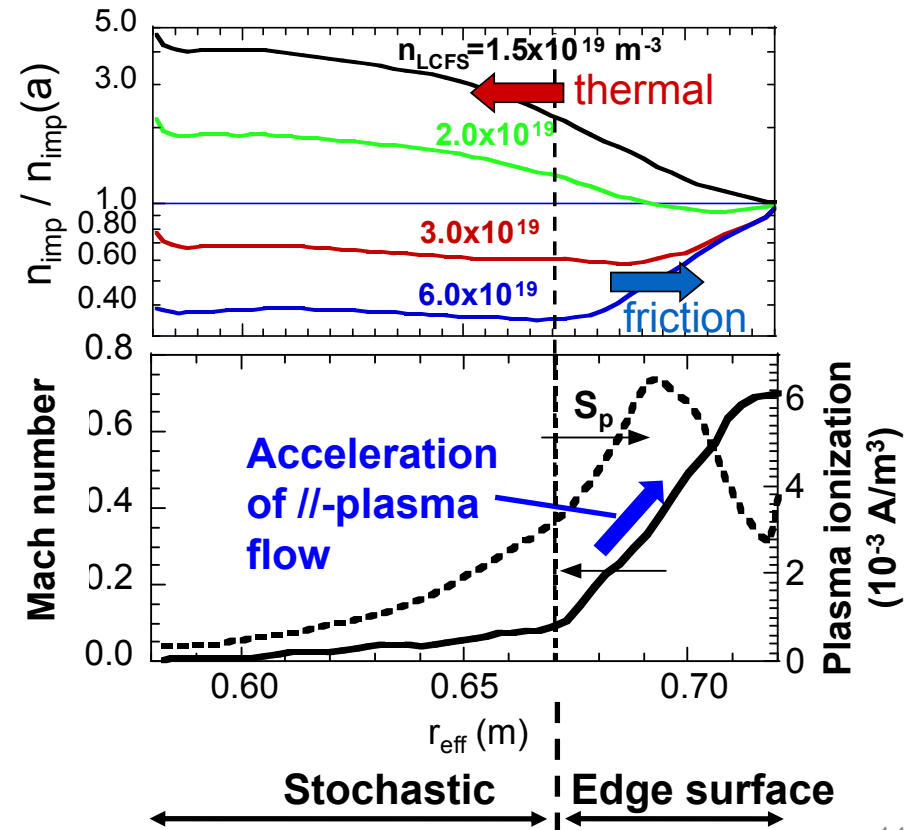
Edge impurity transport in LHD helical divertor

**Numerical analysis of impurity screening in LHD stochastic layer :
high $n \rightarrow$ friction force \uparrow , thermal force $\downarrow \rightarrow$ screening**



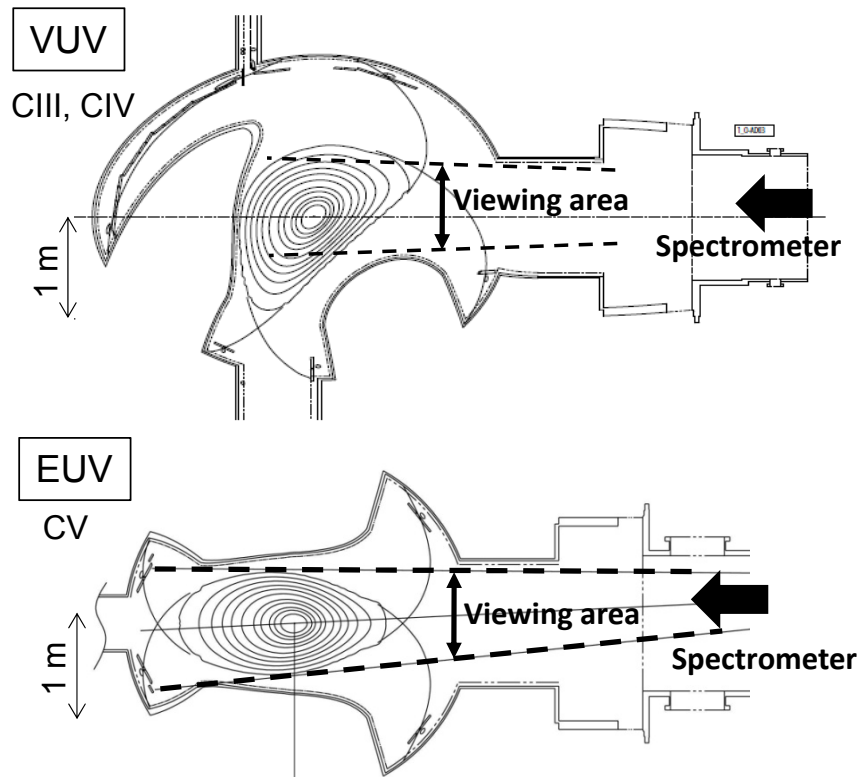
Increasing density

- \rightarrow Enhances friction force in edge surface layer with flow acceleration by short flux tubes
- \rightarrow Suppresses thermal force in stochastic region



Impurity emission measurements and comparison with synthetic diagnostic of EMC3-EIRENE

Qualitative agreement between simulation & experiments



Ionization potential

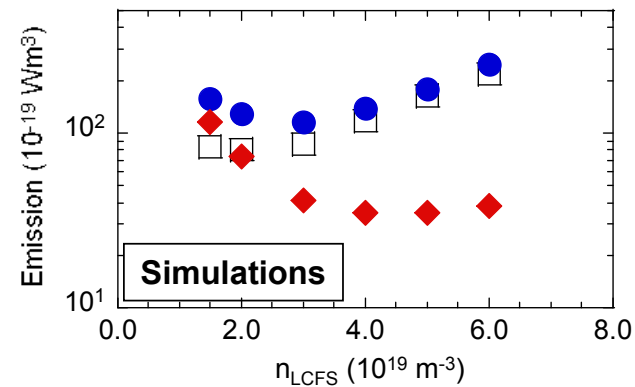
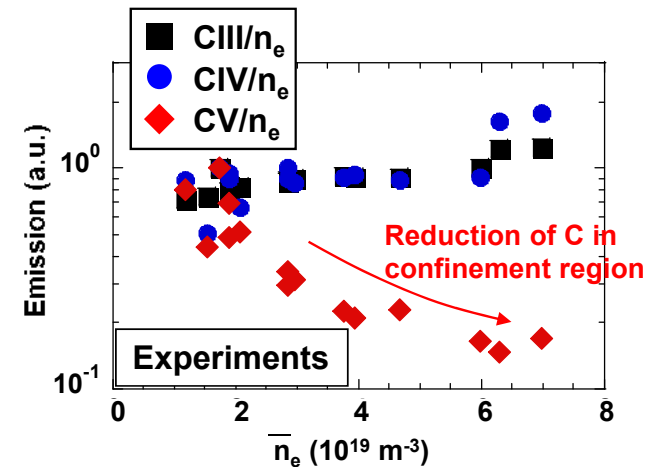
CIII (C^{2+}): 48 eV

CIV (C^{3+}): 65 eV

CV (C^{4+}): 392 eV

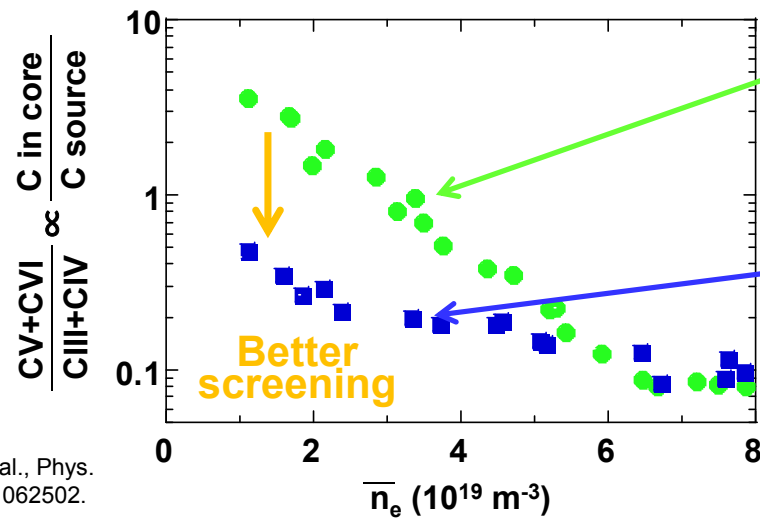
} → Proxy for source

→ Proxy for C in confinement region



SOL thickness dependence of impurity screening: thicker stochastic SOL \rightarrow better screening already at low density

- \triangleright Stochastic layer width (λ_{st}) relative to neutral impurity penetration (λ_{imp})
 $\lambda_{st}/\lambda_{imp} \uparrow \rightarrow$ better screening

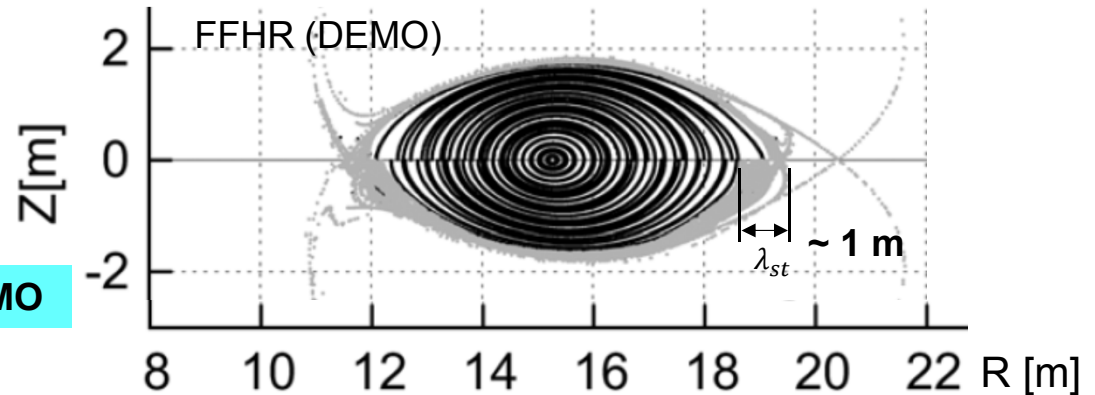
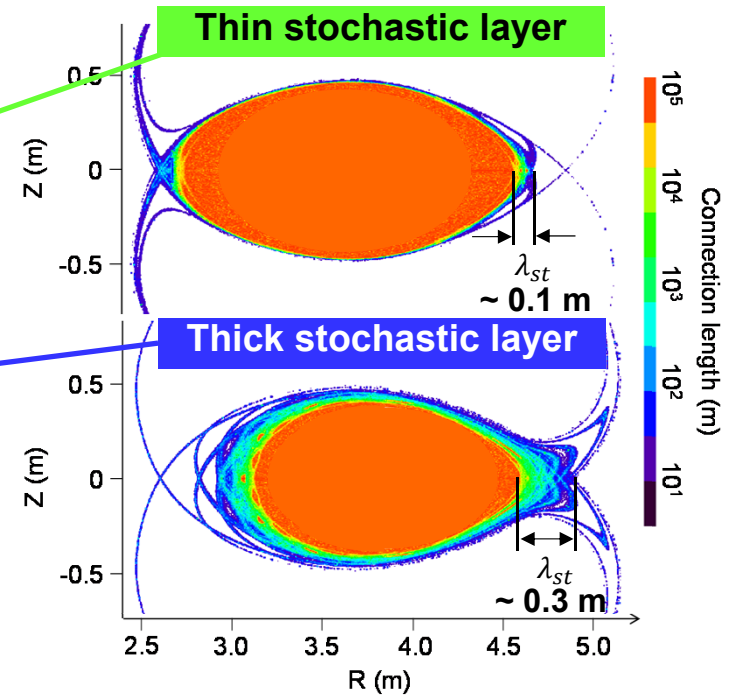


M.B. Chowdhuri et al., Phys. Plasmas **16** (2009) 062502.

In DEMO, stochastic layer width becomes larger, $\lambda_{st} \sim 1\text{m}$, while λ_{imp} (atomic process) remains unchanged.

$$\lambda_{st}/\lambda_{imp} \uparrow\uparrow$$

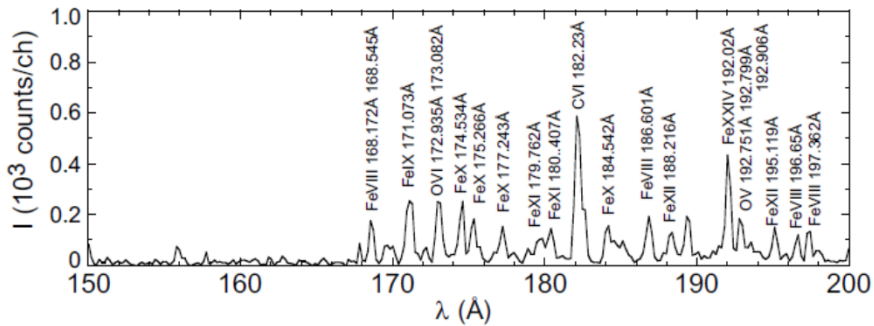
Screening in the stochastic layer can be more effective in DEMO



Impurity screening against high Z materials

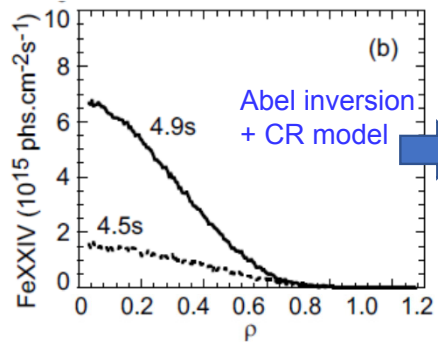
First wall of LHD is stainless steel. However, no significant core iron accumulation is observed.

EUV Spectra of iron emission

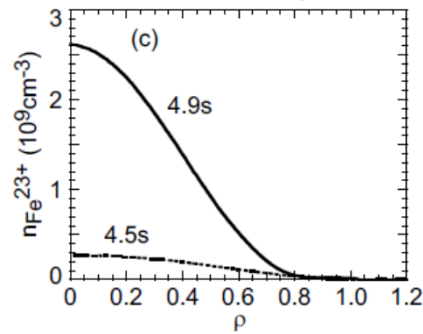


In a frame of edge impurity transport model (friction vs thermal force balance), first ionization potential of impurity is one of key parameters:
Radial position of impurity ion launching \sim mfp of impurity ionization

Line integrated emission profile



Radial profiles of iron density



First ionization potential (eV)

C	Ne	Ar	Fe	W
11.3	21.6	15.8	7.9	7.9

- Further investigation against W is ongoing by replacing divertor plate to W-coated tiles.
- Replacement of one toroidal section (36 degrees) is complete.
- No remarkable impact on core plasma has been observed so far.

Typical iron density in core (EUV & VUV spectroscopy): $< 10^{14} \sim 10^{16} \text{ m}^{-3}$ ($n_{\text{Fe}} / n_e < 10^{-3}$)

Power exhaust in LHD helical divertor

Crude estimation of “AVERAGED” divertor heat load in helical DEMO

“Averaged” divertor heat load: $\Gamma_{\text{div}}^{\text{ave}}$

$$\Gamma_{\text{div}}^{\text{ave}} = P_{\text{div}} / S_{\text{div}}$$

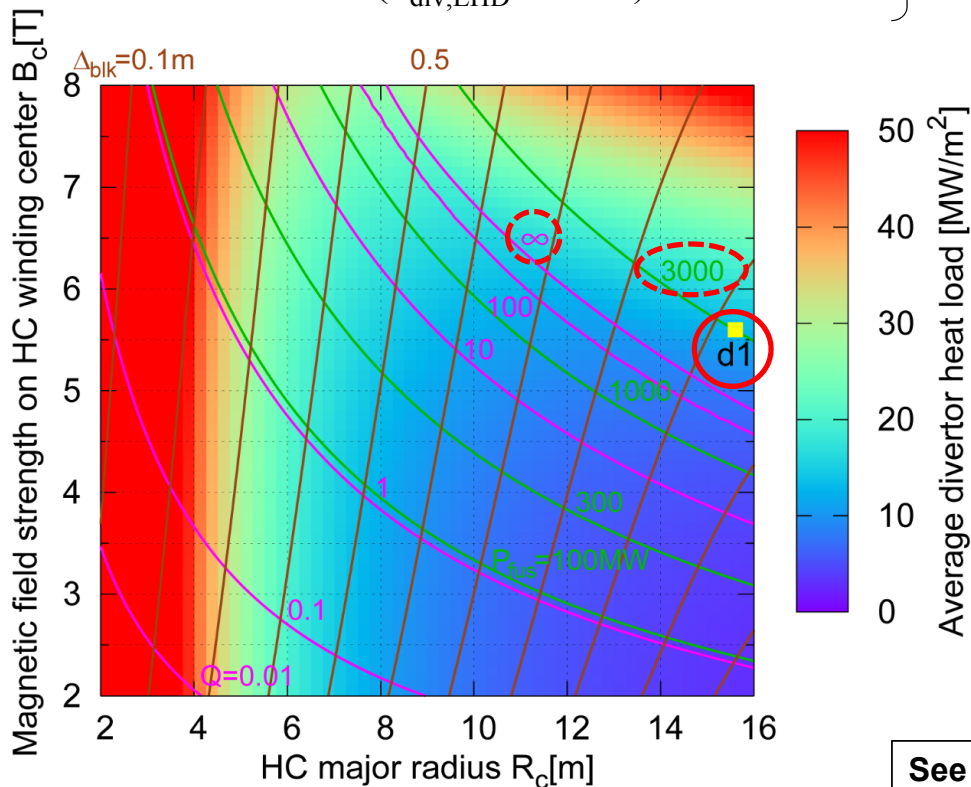
Power to SOL: $P_{\text{div}} (= P_{\alpha} + P_{\text{aux}} - P_{\text{rad}}) = 400$ [MW]

Wetted area: $S_{\text{div}} = S_{\text{div,LHD}} (R_c / R_{c,\text{LHD}})^2$
 ($S_{\text{div,LHD}} = 2$ m²)

$$\Gamma_{\text{div}}^{\text{ave}} \sim 13 \text{ MW/m}^2$$

The local maximum can be several times larger due to the non-uniformity in helical direction.

Needs heat load mitigation



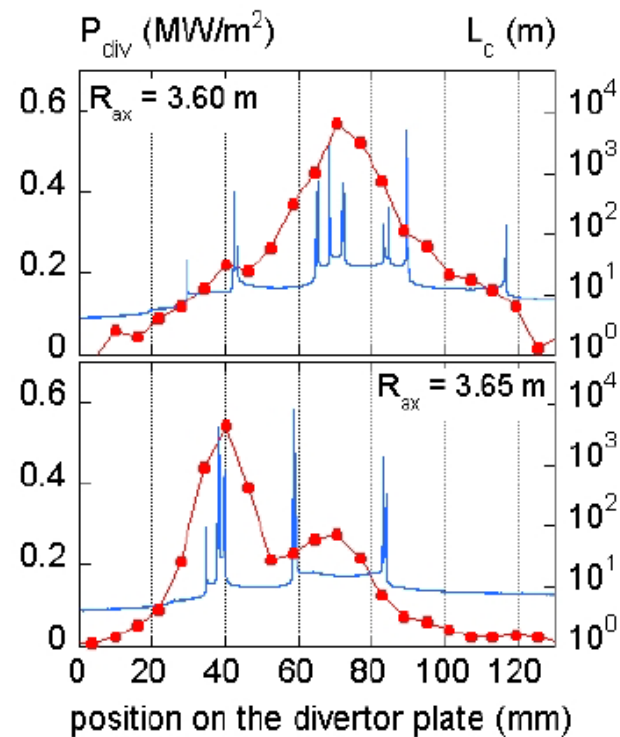
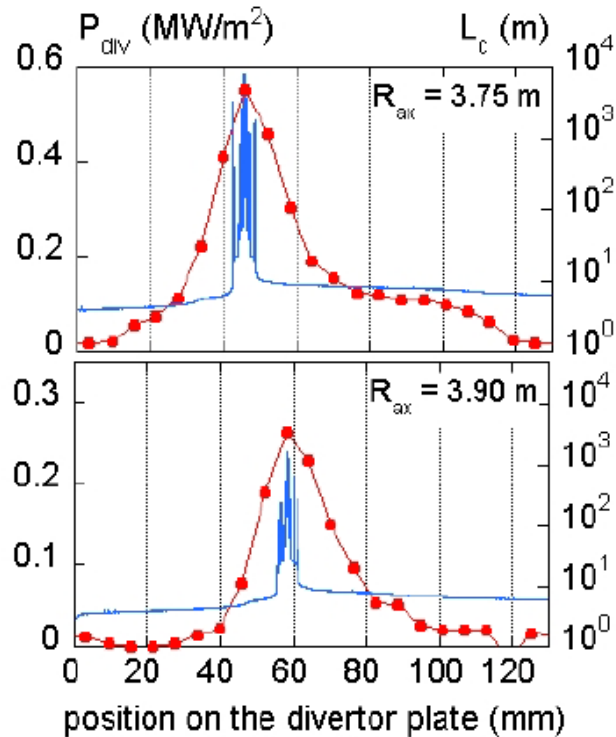
	FFHR-d1 (DEMO)
R / a [m]	15.6 / 2.5
B_c [T]	~5
P_{fus} [MW]	3000
$f_{\text{He}} / f_{\text{Ar}}$ [%]	5 / 0
P_{rad} [MW]	200
P_{aux} [MW]	0
$P_{\text{div}} (= P_{\alpha} + P_{\text{aux}} - P_{\text{rad}})$ [MW]	400
P_{div} / R [MW/m]	35

See [46] T. Goto (M. Kobayashi)

Divertor foot-prints of magnetic flux tubes & power load in various configurations

Single peak : Good correlation between long flux tubes and peak power load.

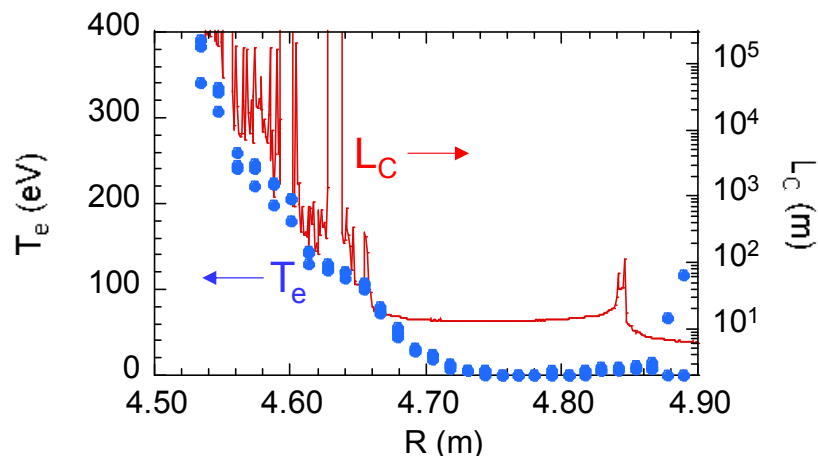
Multi-peak : foot-print width becomes broad, power peak does not necessarily correlate with L_c peak.



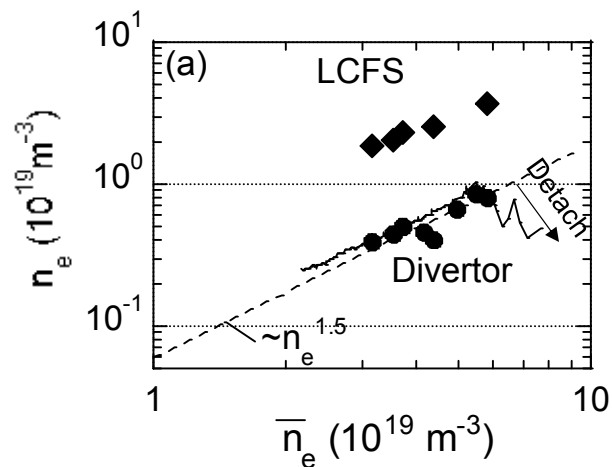
Multi-peak strike lines could widen the wetted area.

Edge magnetic field structure, plasma parameter profiles, and impurity radiation

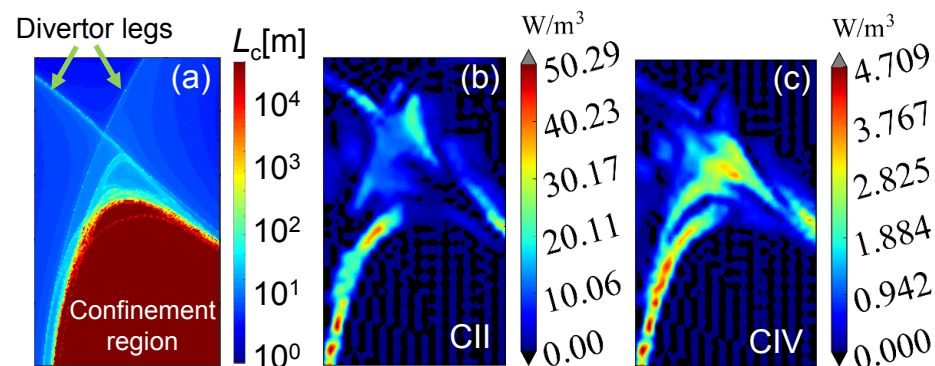
L_C changes from a few meters to more than 1km.
 T_e ranges from a few tens to a few hundreds eV.



Density around LCFS is larger than at the divertor region.



Tomographic inversion of carbon emission



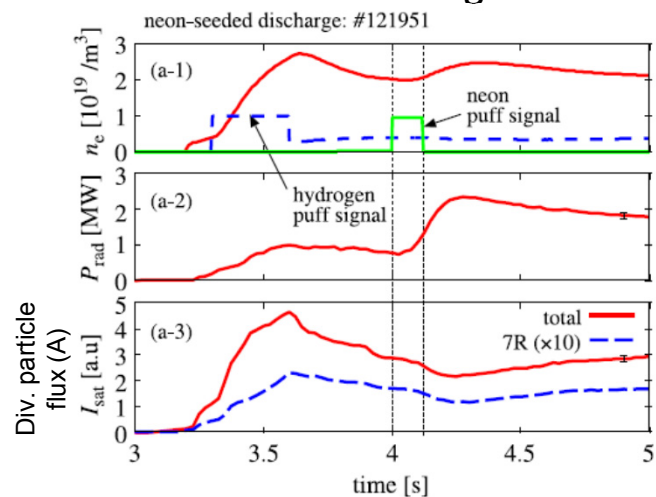
Impurity radiation: the stochastic layer > divertor region

T. Kobayashi et al. NME **19** (2019) 239.

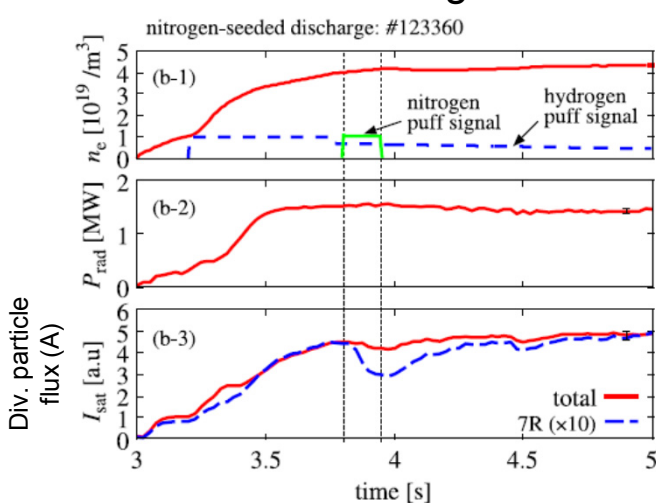
The edge stochastic layer has potential of various impurity emissions of different charge states.

Impurity seeding experiments: Ne and N

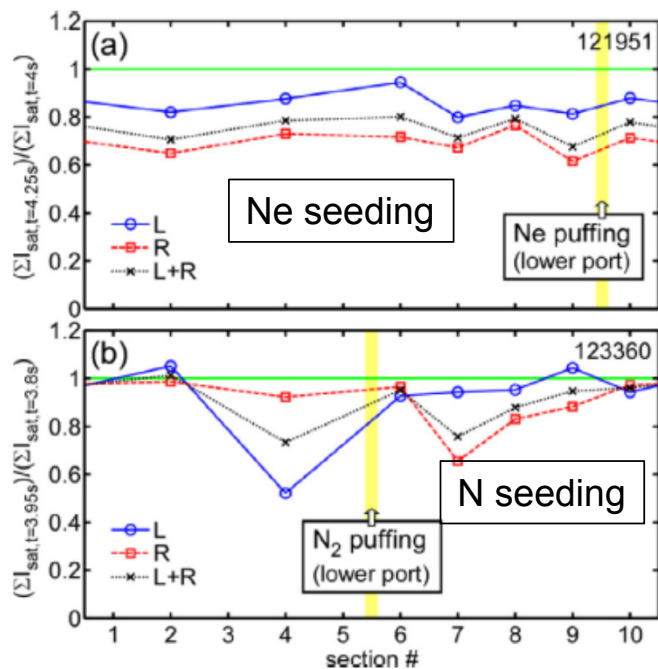
Ne seeding



N seeding



Toroidal profile of div. particle flux



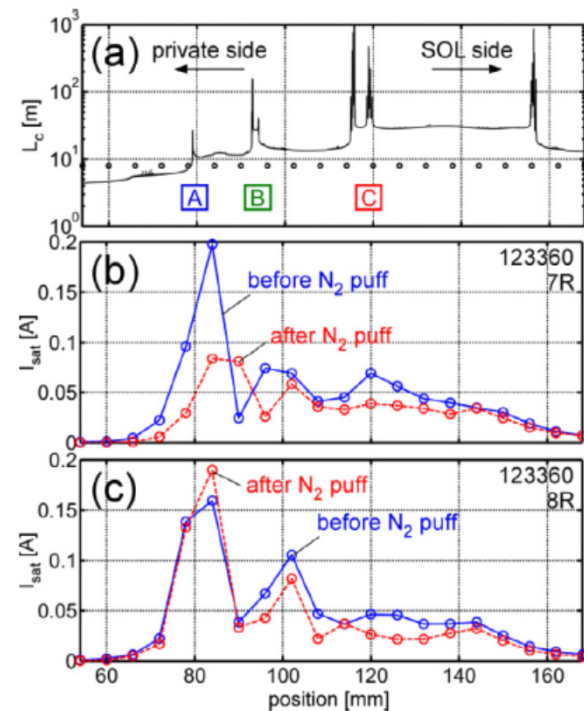
Ne: Toroidally uniform reduction
N: Toroidally asymmetric profile

H. Tanaka et al. NME 12 (2017) 241.

Sustainment of detached phase for longer duration is still to be explored.

For recent experiments with mixture seeding Ne + Kr, see [48] K. Mukai

L_C & div particle flux profile at div plate (N seeding)

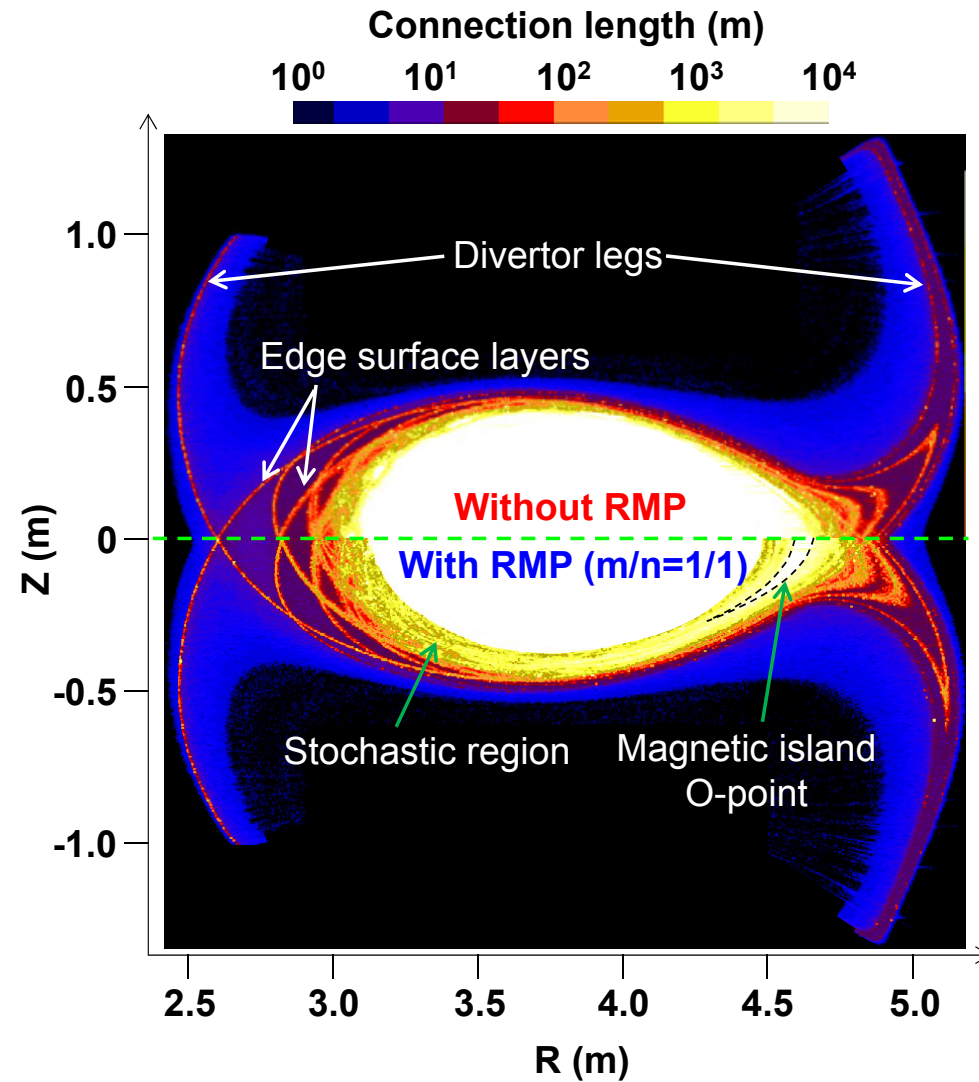
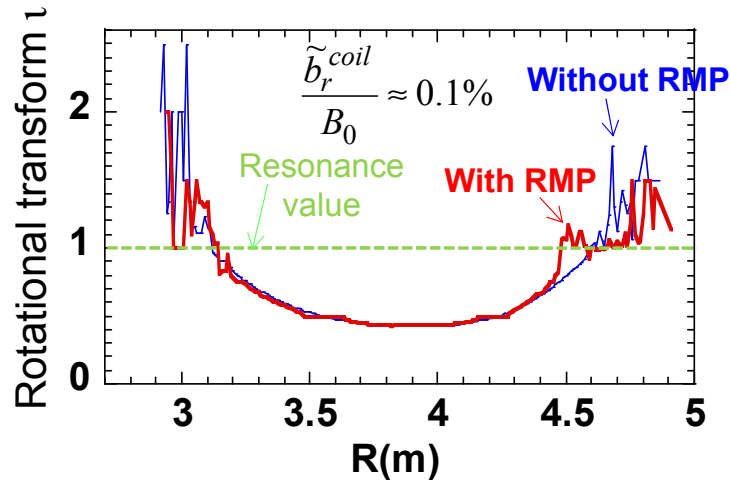
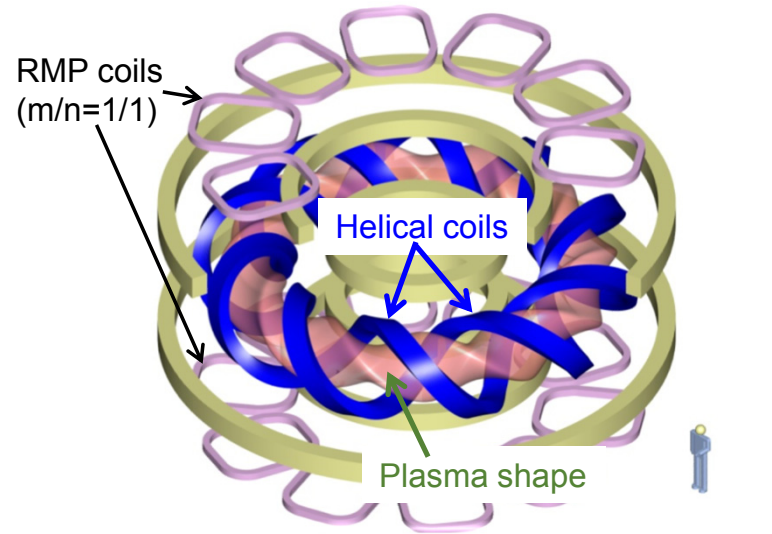


In N seeding, div flux reduction is strongly affected by L_C structure.

G. Kawamura et al. PPCF 60 (2018) 084005.
K. Mukai et al. NF 55 (2015) 083016.

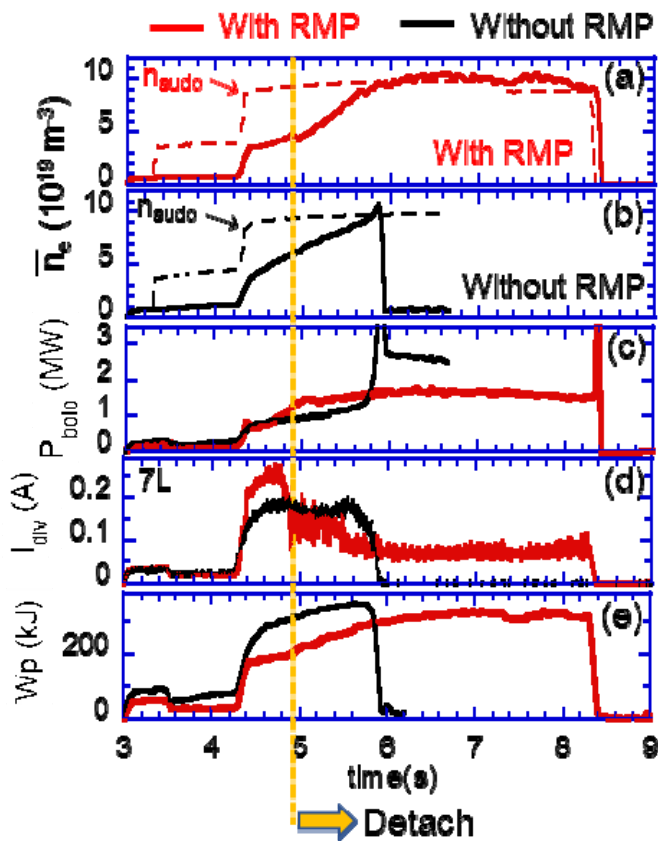
Detachment control with RMP application

$R = 3.9 \text{ m}$, $\bar{a} \sim 0.7 \text{ m}$, 10 field periods (toroidal)
 Divertor : carbon, First wall : Stainless steel

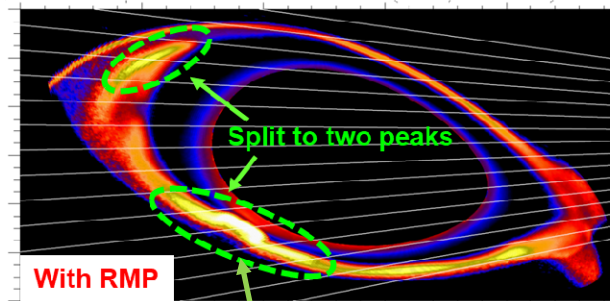
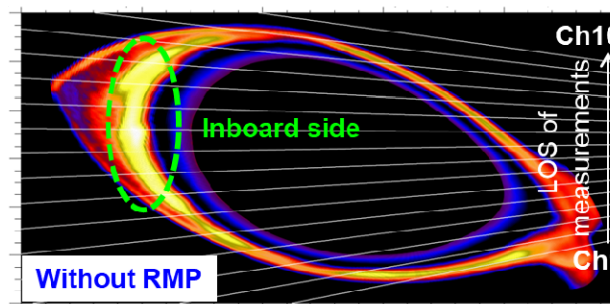


With RMP → Stable sustainment of radiative divertor operation
Without RMP → Radiation collapse due to thermal instability

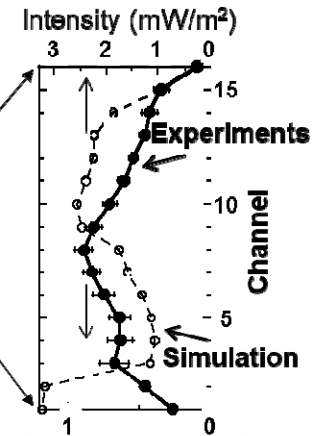
Application of RMP leads to stable sustainment of detached plasma near density limit.



Carbon radiation distribution by EMC3-EIRENE

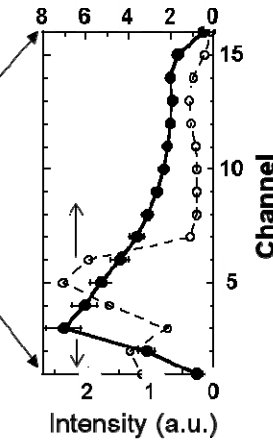


X-point of m/n=1/1 island



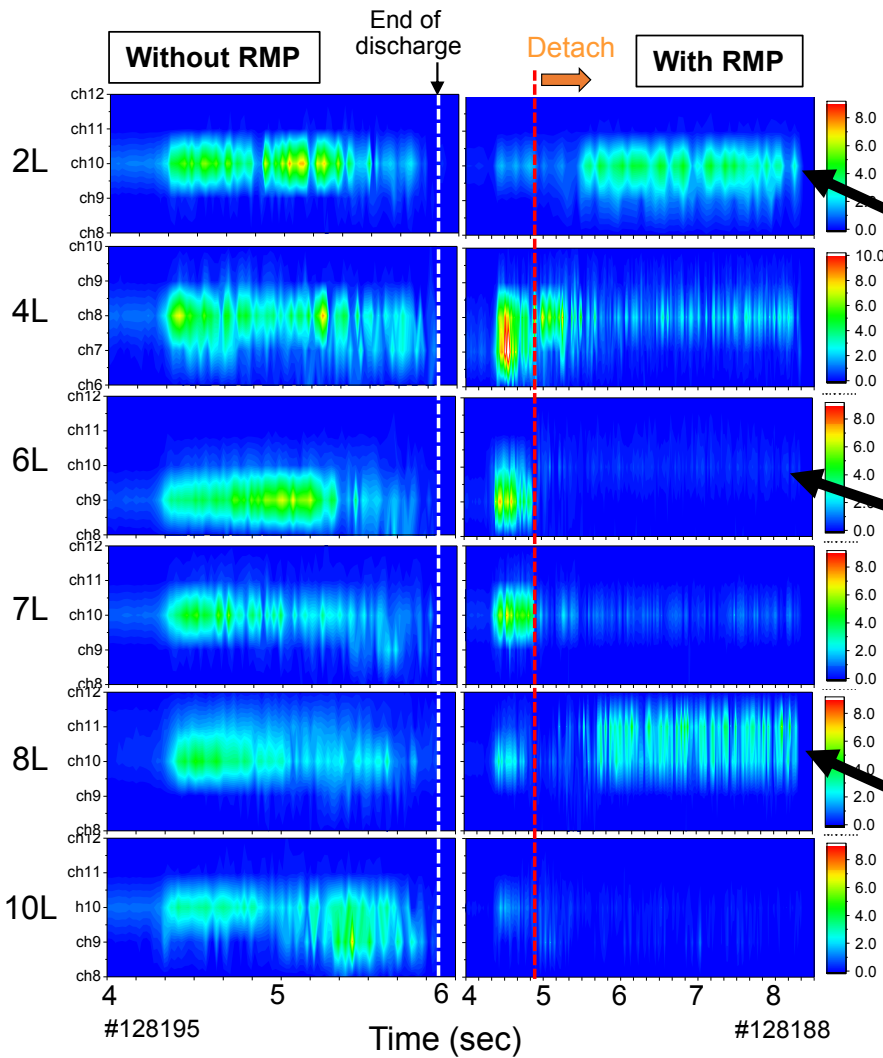
➤ The radiation profile qualitatively agrees between experiments & simulation.

➤ Results implies selective cooling at X-point of m/n=1/1 island in experiments.

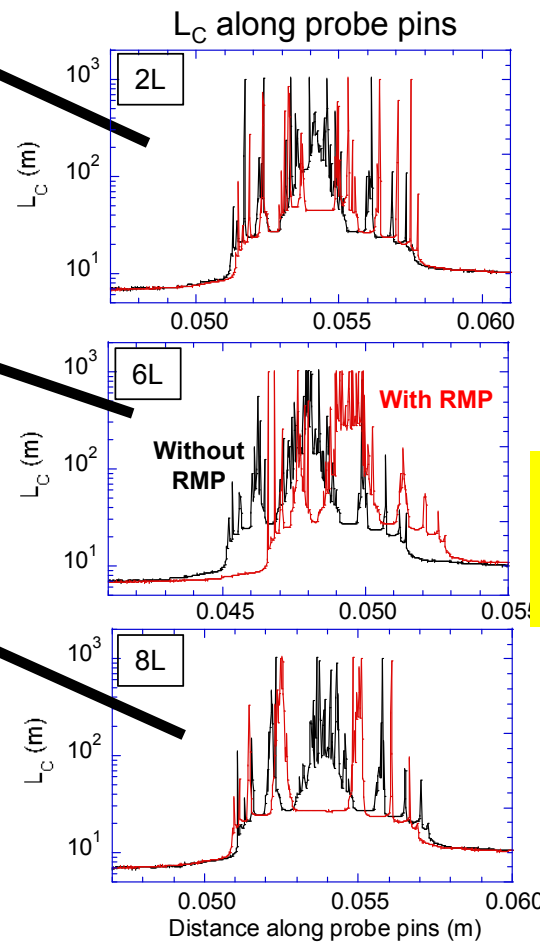


➤ The magnetic island structure "catches" the radiation and prevents it from penetrating inward?!

Divertor heat load distributions (Langmuir probe): attached & detached phases



- Nearly uniform toroidal distribution without RMP
- ➔ Toroidal modulation with RMP due to change of L_C



- After detachment transition, heat load decreases at most of divertor plates (HYDROGEN).
- Slight increase is observed at certain sections (2L, 8L), where L_C profile is split by RMP.



➤ In DEUTERIUM plasma, heat load decreases at all toroidal sections at detachment. Isotope effects? Or due to amount of carbon?

Summary

The LHD heliotron divertor needs to be optimized toward helical DEMO

Advantage (Control of transport)



Disadvantage (Complexity of transport & engineering)

- Effective impurity screening with stochastic layer
To be confirmed for high-Z impurity
- Flexibility of edge magnetic field structure
Thicker stochastic layer → better screening
Controllability of detachment

- Neutral compression
Further improvement is foreseen in next experiments
(could be improved in DEMO)
- Non-uniform heat deposition on divertor plates
Needs of development of energy dissipation scheme
- Technological challenge in complex 3D shaping
Pumping, magnet system etc.

What is the most critical issues toward helical DEMO among above issues?